Bokeh Diffusion: Defocus Blur Control in Text-to-Image Diffusion Models

ARMANDO FORTES, S-Lab, Nanyang Technological University, Singapore TIANYI WEI, S-Lab, Nanyang Technological University, Singapore SHANGCHEN ZHOU, S-Lab, Nanyang Technological University, Singapore XINGANG PAN, S-Lab, Nanyang Technological University, Singapore



Bokeh range: 0-30

Continuous bokeh generation

Fig. 1. Bokeh Diffusion enables precise, scene-consistent bokeh control in text-to-image diffusion models. Top Left: Images are conditioned on an explicit blur parameter to generate outputs ranging from sharp to strongly defocused. Top Right: Our method maintains consistent scene content across different blur level conditions. Bottom: Continuous adjustment of blur strength produces smooth transitions across the bokeh range.

Recent advances in large-scale text-to-image models have revolutionized creative fields by generating visually captivating outputs from textual prompts; however, while traditional photography offers precise control over camera settings to shape visual aesthetics-such as depth-of-field via aperturecurrent diffusion models typically rely on prompt engineering to mimic such effects. This approach often results in crude approximations and inadvertently alters the scene content. In this work, we propose Bokeh Diffusion, a scene-consistent bokeh control framework that explicitly conditions a diffusion model on a physical defocus blur parameter. To overcome the scarcity of paired real-world images captured under different camera settings, we introduce a hybrid training pipeline that aligns in-the-wild images with synthetic blur augmentations, providing diverse scenes and subjects as well as supervision to learn the separation of image content from lens blur. Central to our framework is our grounded self-attention mechanism,

Authors' addresses: Armando Fortes, S-Lab, Nanyang Technological University, Singapore, armandol001@ntu.edu.sg; Tianyi Wei, S-Lab, Nanyang Technological University, Singapore, tianyi.wei@ntu.edu.sg; Shangchen Zhou, S-Lab, Nanyang Technological University, Singapore, sczhou@ntu.edu.sg; Xingang Pan, S-Lab, Nanyang Technological University, Singapore, xingang.pan@ntu.edu.sg.

trained on image pairs with different bokeh levels of the same scene, which enables blur strength to be adjusted in both directions while preserving the underlying scene. Extensive experiments demonstrate that our approach enables flexible, lens-like blur control, supports downstream applications such as real image editing via inversion, and generalizes effectively across both Stable Diffusion and FLUX architectures. Project page: this https URL.

CCS Concepts: • Computing methodologies → Computer vision; Image manipulation; Neural networks; • Applied computing → Media arts.

Additional Key Words and Phrases: Image Synthesis, Controllable Generation, Diffusion Models

1 INTRODUCTION

Photography has long offered a rich set of camera controls for shaping visual aesthetics. By varying the lens aperture and focal distance, photographers can decide whether a scene appears deeply in focus or softly blurred in the foreground or background [Langford et al. 2015]. In professional workflows, these lens-based adjustments are



Fig. 2. State-of-the-art text-to-image models [Labs 2024] do not understand textual photographic cues, and unintentionally alter image composition.

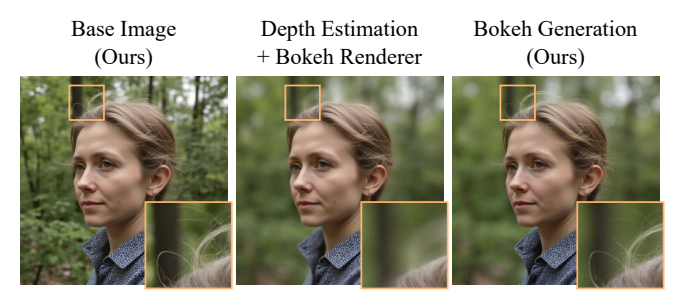


Fig. 3. Comparison between our generative method and BokehMe [Peng et al. 2022], which depends on external depth estimation.

integral to crafting the photograph's mood and composition [Free-man 2007]. Yet, in the rapidly evolving domain of text-to-image (T2I) generation, reproducing such camera effects is surprisingly difficult. Existing approaches typically rely on *prompt engineering* (e.g., adding "f/1.8 aperture" to the text prompt), which often yields inaccurate approximations and unintentionally alters the scene content. As a result, changing apertures might yield not just a different bokeh but an entirely different object arrangement (see Fig. 2).

Recent works have started to explore controlling camera intrinsics in image generation via camera tokens [Fang et al. 2024], but often still entangle depth-of-field with content changes. Others model camera settings along the temporal axis of a text-to-video framework to improve consistency [Yuan et al. 2024], requiring the generation of up to 7 frames per prompt at inference for stronger results. This introduces substantial computational overhead and redundancy, particularly when only a single bokeh level is needed, and makes the approach not directly compatible with state-of-the-art T2I models. Moreover, despite the increased complexity, we find it still struggles to preserve fine scene details across large bokeh transitions.

In contrast, we propose a method for scene-consistent bokeh control directly within the T2I paradigm, offering greater efficiency and flexibility while fully leveraging the generative power of modern T2I backbones. A key obstacle is that real-world images with paired camera settings for the same scene (e.g., identical viewpoint at f/1.8 and f/16) are scarce. To address this, we align in-the-wild photographs (with lens-related metadata) and synthetic blur augmentations, allowing the model to learn from both authentic lens blur across diverse settings and structured focus—defocus pairs. Through this hybrid data pipeline, our model learns to better disentangle scene content from depth-of-field while closely mimicking lens-based defocus blur. Beyond dataset design, our framework conditions the

diffusion process on a physical bokeh parameter and employs specialized attention mechanisms to preserve scene layout. Specifically, we use lightweight cross-attention adapters to inject blur cues into the model, allowing fine-grained bokeh adjustments. Additionally, our *grounded self-attention* is trained with image pairs, ensuring that changes in blur level respect the scene composition from a single reference image. This design significantly improves content preservation during bokeh manipulation—a key challenge in controllable image synthesis—letting us smoothly transition between deep and shallow depth-of-field without reshaping the scene.

Compared to post-processing approaches that add blur to images based on estimated depth maps [Peng et al. 2022], our method offers several key advantages. First, it allows direct bokeh control during generation, letting users specify blur strength without post-processing. Second, given a generated image, our method supports adjusting the bokeh strength in both directions—either increasing or decreasing it—whereas post-processing methods struggle to remove blur. Third, by leveraging the generative prior of the pretrained diffusion model and our hybrid dataset, our method produces more natural bokeh effects, especially in challenging areas such as thin structures and translucent materials (see Fig. 3 and Fig. 9).

In summary, (1) we propose Bokeh Diffusion, a scene-consistent bokeh control framework for T2I diffusion, allowing physically motivated defocus blur changes without altering scene content; (2) we introduce a curated dataset and hybrid training pipeline leveraging EXIF-based cues from in-the-wild data and synthetic blur augmentations to furnish the model with contrastive examples; (3) we extensively evaluate our method and show that it consistently outperforms both pretrained and finetuned baselines across accuracy, consistency, and perceptual quality metrics; (4) we demonstrate the versatility of our approach by deploying it on both the UNetbased Stable Diffusion and the MMDiT-based FLUX architectures, achieving strong results across both; and (5) we explore additional applications such as real image editing via inversion.

2 RELATED WORK

2.1 Text-to-image diffusion.

Diffusion models [Ho et al. 2020; Sohl-Dickstein et al. 2015] have become the dominant approach in text-to-image (T2I) generation due to their high sample quality and diversity. Early works such as GLIDE [Nichol et al. 2022] introduced text-conditioned diffusion with a cascaded architecture for improved resolution. Stable Diffusion [Rombach et al. 2022] shifted generation to a lower-dimensional latent space, enabling efficient high-resolution synthesis. Other prominent works include [Bao et al. 2023b; Chen et al. 2024a, 2023; Podell et al. 2023; Saharia et al. 2022]. More recently, Stable Diffusion 3 [Esser et al. 2024] and FLUX [Labs 2024] have set a new state-of-the-art, by scaling diffusion transformer [Bao et al. 2023a; Peebles and Xie 2023] backbones with rectified flows [Lipman et al. 2022; Liu et al. 2022]. Despite their advancements in prompt fidelity and scene composition, these models struggle with fine-grained photographic controls, such as depth-of-field manipulation.

Other recent works have also explored enhancing controllability in diffusion models. DreamBooth [Ruiz et al. 2023] enables subject-driven generation, while ControlNet [Zhang et al. 2023]

incorporates structural conditions like pose or edge maps. T2I-Adapter [Mou et al. 2023] and IP-Adapter [Ye et al. 2023] facilitate reference image-driven generation. Further studies reveal that selfand cross-attention layers encode structural and semantic information, which has been leveraged for editing [Cao et al. 2023; Hertz et al. 2022], style adaptation [Hertz et al. 2024; Wang et al. 2024b], and appearance transfer [Alaluf et al. 2024].

Camera-conditioned diffusion models. 2.2

Most existing works on camera control in diffusion models focus on extrinsic parameters, such as camera position and viewing angle [Cheng et al. 2024; Höllein et al. 2024; Kumari et al. 2024], or trajectory in video generation [He et al. 2024; Sun et al. 2024; Wang et al. 2023b; Xiao et al. 2025, 2024b]. Regarding intrinsic camera control, Voynov et al. [2024] explore conditioning T2I diffusion on diverse optical geometries to simulate lens-induced distortions. Additionally, some methods model zoom implicitly [Cheng et al. 2024; Wang et al. 2024a], while others perform prompt-based conditioning on camera settings [Fang et al. 2024; NVIDIA et al. 2024].

Camera Settings as Tokens (CSaT) [Fang et al. 2024] is a pioneering approach that introduces explicit conditioning on intrinsic parameters like aperture. However, it does not enforce scene consistency (i.e., altering the aperture often results in significant scene changes). While pairing CSaT with ControlNet [Zhang et al. 2023] improves structural guidance, it does not guarantee consistent finegrained scene content. Generative Photography [Yuan et al. 2024] addresses scene consistency more directly by modeling intrinsic camera control along the temporal axis of a text-to-video (T2V) model. However, it depends on T2V's temporal modules and requires constantly generating several frames during inference, increasing computational overhead and limiting flexibility for single-image generation or editing. In contrast, our method achieves scene-consistent bokeh control entirely within the T2I paradigm. This allows our approach to be directly applied to state-of-the-art T2I models with stronger generative capability, avoid the overhead and redundancy of multi-frame inference, and support efficient, scalable deployment in both generation and editing workflows.

3 **METHOD**

3.1 Background

Diffusion models. Diffusion models [Ho et al. 2020; Sohl-Dickstein et al. 2015] learn to synthesize data samples from Gaussian noise. In the forward process, diffusion models gradually add noise to the data $x_0 \sim q(x_0)$, formalized by a Markov chain:

$$q(x_{1:T}|x_0) = \prod_{t=1}^{T} q(x_t|x_{t-1}), \qquad (1)$$

$$q(x_t|x_{t-1}) = \mathcal{N}\left(x_t; \sqrt{\alpha_t}x_{t-1}, \beta_t \mathbf{I}\right), \tag{2}$$

where β_t is the noise schedule and $\alpha_t = 1 - \beta_t$.

In the reverse process, data is synthesized by a Gaussian model that learns to approximate the denoising step:

$$p_{\theta}\left(x_{t-1}|x_{t}\right) = \mathcal{N}\left(x_{t-1}; \mu_{\theta}\left(x_{t}, t\right), \sigma_{t}^{2} I\right). \tag{3}$$

The mean $\mu_{\theta}(x_t, t)$ can be derived to learn a noise prediction network ε_{θ} , which is often trained with MSE loss:

$$\min_{\theta} \quad \mathbb{E}_{t,x_{0},\varepsilon} \| \varepsilon - \varepsilon_{\theta} \left(x_{t},t \right) \|_{2}^{2}, \tag{4}$$

where $x_t = \sqrt{\overline{\alpha}_t} x_0 + \sqrt{1 - \overline{\alpha}_t} \varepsilon$ and $t \sim \{1, 2, ..., T\}$.

For conditional generation, we model the distribution $q(x_0|c)$. The noise prediction network can be adapted by incorporating the condition c during training, typically via the attention mechanism.

3.1.2 Attention mechanism in T2I diffusion. Formally, attention can be expressed as a weighted sum of values V, with weights determined by the compatibility between a query *Q* and keys *K*:

Attention
$$(Q, K, V) = \text{Softmax}\left(\frac{QK^{\top}}{\sqrt{d}}\right)V.$$
 (5)

In most T2I diffusion models [Chen et al. 2024a, 2023; Podell et al. 2023; Rombach et al. 2022; Saharia et al. 2022], Q is projected from the spatial features, while K and V are projected either from the same spatial features (self-attention) or from text embeddings (crossattention). Overall, these layers hold substantial information about the structure and content, allowing diffusion models to maintain coherent layouts while generating contextually relevant details.

3.1.3 Thin lens model. As a camera captures a scene onto a 2D imaging plane, some parts may be in focus and others not. Given a circular aperture, the image of any point source not located at the focal distance is a small disk. This disk is often referred to as the circle of confusion (CoC), and its diameter d depends on the scene and camera settings [Lagendijk and Biemond 2009; Wang et al. 2023a]. Specifically, d can be calculated by:

$$d = \frac{f^2}{N(S_1 - f)} \frac{|S_2 - S_1|}{S_2},\tag{6}$$

where f is the focal length, N is the aperture (i.e., F-number), S_1 is the focus distance, S_2 is the subject distance.

3.1.4 Defocus blur rendering. In blur rendering methods [Peng et al. 2021; Yang et al. 2016], the idea is to scatter each pixel in its neighboring areas where the distance between them is less than its blur radius. As discussed in [Peng et al. 2022; Wadhwa et al. 2018; Yang et al. 2016], given the disparity of a pixel, its blur radius is:

$$r = K \cdot \Delta disp, \quad \Delta disp = \left| \frac{1}{S_1} - \frac{1}{S_2} \right|.$$
 (7)

Such methods are capable of rendering realistic bokeh effects in depth-continuous areas but they tend to suffer from color-bleeding artifacts at depth discontinuities [Peng et al. 2022]. Recent rendering methods mainly focus on improving this limitation, e.g., using neural renderers to fix erroneous areas [Peng et al. 2022], or layered occlusion-aware bokeh rendering [Sheng et al. 2024].

3.2 Leveraging In-the-wild Image Augmentation

In principle, real photographs with naturally occurring lens blur provide the most faithful representation of defocus blur in varied scenes. However, major limitations arise when relying exclusively on in-the-wild (ITW) data. First, images of the same scene captured at multiple camera settings (e.g., identical viewpoint at f/1.8 and f/16) are exceedingly rare. Consequently, the model can struggle

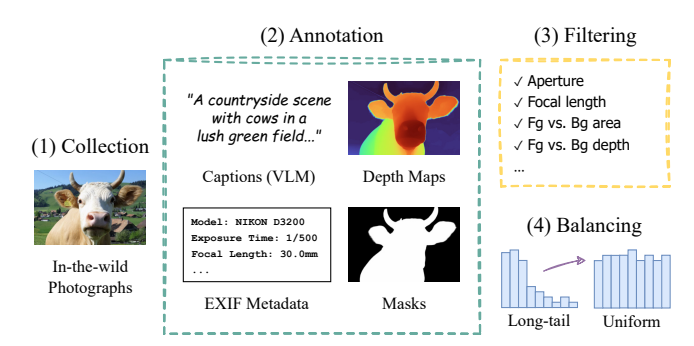


Fig. 4. Data collection and curation pipeline.

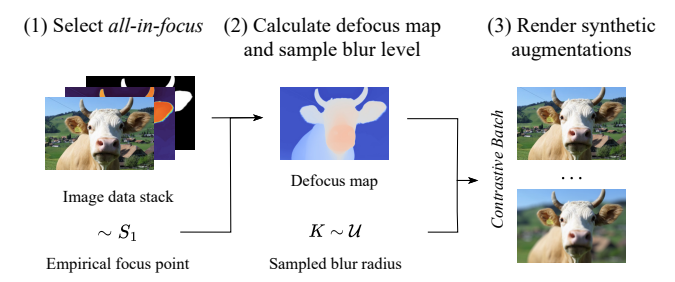


Fig. 5. In-the-wild image augmentation.

to disentangle the defocus blur from the underlying scene arrangement, leading to local minima. Second, real images often exhibit shooting preference bias (e.g., portrait photographers opting for wide apertures, landscape photographers going for narrow ones). While there do exist datasets with multi-aperture captures of the same scene [Abuolaim and Brown 2020; Ignatov et al. 2020; Zhang et al. 2019], they are typically small in scale due to the manual effort required for such data collection. Moreover, these datasets tend to focus on static, inanimate scenes, since capturing precisely aligned shots with varying apertures is difficult when dynamic elements (e.g., people or animals) are present. This limited diversity makes them less suitable for training a generative model that must generalize across varied subjects, environments, and compositions.

To address these challenges, we build a hybrid training pipeline combining two complementary data sources. First, we curate a collection of in-the-wild photographs enriched with lens metadata, which offers diverse content and authentic photographic blur across many scenes (Sec. 3.2.1). Second, we apply synthetic defocus blur augmentations to nearly all-in-focus images [Yuan et al. 2024] using a fast bokeh rendering engine [Peng et al. 2022] (Sec. 3.2.2) for contrastive image pairs. This strategy enables the model to learn realistic defocus in diverse settings while also acquiring supervision to disentangle blur from the scene.

3.2.1 In-the-wild images (Fig. 4). We curate a dataset of in-the-wild photographs from Flickr¹². We select images licensed under public-domain-friendly terms, and annotate each image with (a) estimated depth maps using Bochkovskii et al. [2024], (b) foreground masks produced via Zheng et al. [2024], (c) EXIF metadata, and (d) text

captions from multiple VLMs [Chen et al. 2024b,c; Xiao et al. 2024a]. We filter out images lacking reliable lens info, unreasonable foreground area, small depth range, *etc.* Finally, we perform balancing based on our physical defocus blur annotation obtained from the EXIF metadata. This step mitigates the strong long-tail bias in real photographs, providing a more uniform representation. The resulting dataset has around 15K samples, of which around 10% are nearly all-in-focus and used for synthetic blur augmentation.

3.2.2 Synthetic blur augmentation (Fig. 5). We synthesize additional defocus examples by rendering artificial blur on nearly all-in-focus images using BokehMe [Peng et al. 2022]. Specifically, we estimate a per-pixel disparity map and then sample a blur parameter K to generate contrastive "focus—defocus" states of the same image. These image pairs help the model avoid local minima by providing direct evidence that the same object layout can appear either sharp or defocused, and they are also essential for training our grounded self-attention module, introduced in the following sections. Moreover, synthetic rendering allows us fine-grained control over the bokeh distribution as it allows us to continuously sample from the camera parameter space, unlike real datasets which are often constrained to a few discrete aperture settings.

3.2.3 Mixed dataset training. In practice, combining real ITW images with synthetic bokeh augmentations provides an effective balance. To this end, it is necessary to ensure that bokeh conditioning is consistent across both data sources. As discussed in Sec. 3.1.3, real-lens defocus can be estimated via the CoC diameter d from the thin lens model, while synthetic blur rendering often uses a scalar K as the pixel blur radius per unit disparity (7). Rewriting the CoC expression in terms of $\Delta disp$, the dependency on S_2 can be factored out. This yields a blur diameter proportional to disparity difference:

$$d = \frac{f^2 S_1}{N(S_1 - f)} \cdot \Delta disp,\tag{8}$$

which matches the linear disparity formulation used in synthetic rendering. Converting d to a radius, the corresponding synthetic blur strength in the pixel space can be approximated by:

$$K \approx \frac{f^2 S_1}{2N(S_1 - f)} \times \text{pixel_ratio},$$
 (9)

where f and N are obtained from EXIF metadata, S_1 is calculated based on heuristics, and $pixel_ratio$ accounts for different camera sensor sizes and image resolution. This formulation allows us to compute a physically grounded blur parameter K for real images, aligned with the synthetic rendering domain. As a result, we can train the model using a unified defocus representation.

3.3 Defocus Blur Conditioning

Inspired by previous work [Ye et al. 2023], we employ decoupled cross-attention to inject our defocus blur condition into the existing T2I diffusion pipeline. Specifically, for each cross-attention layer in the decoder of the UNet, we add a new pair of key-value projections W_k' , W_v' tied to a lightweight bokeh feature c_b . This feature is obtained by passing the scalar defocus parameter through a small MLP. The original text-based keys and values (K, V) remain frozen. Meanwhile, the new bokeh cross-attention is computed with the

¹https://www.flickr.com/

²madebyollin/megalith-10m

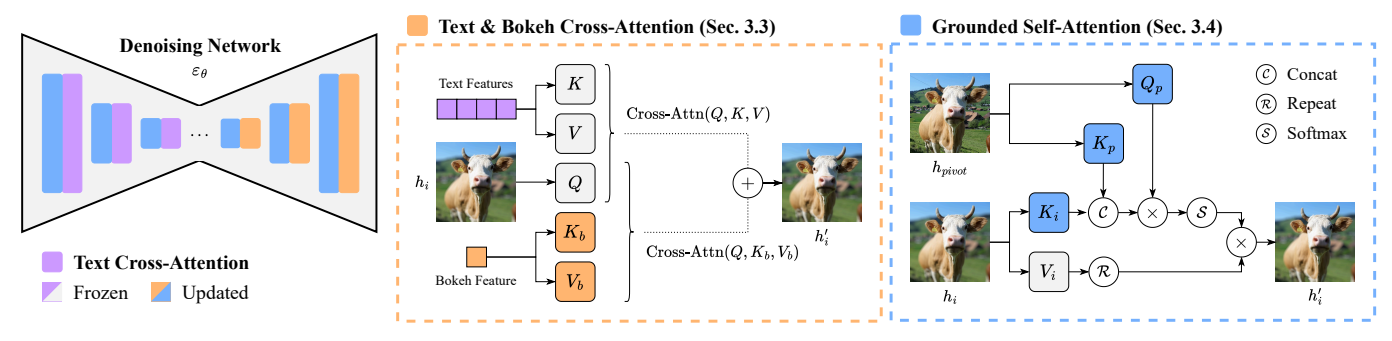


Fig. 6. Overview of Bokeh Diffusion's conditioning and scene-consistency mechanisms. Bokeh Cross-Attention (Sec. 3.3), applied at deeper layers of the text-to-image diffusion model, injects a defocus conditioning signal, decoupled from semantic guidance. Grounded Self-Attention (Sec. 3.4) ensures fine-grained scene consistency across different defocus levels, where the pivot image's queries anchor the scene structure, while shared keys allow the model to disentangle defocus blur from scene composition.

same query Q but keys and values $K_b = c_b W_b^k$, $V_b = c_b W_b^v$, then linearly combined with the text cross-attention output:

$$h^{\text{new}} = \underbrace{\text{Attention}(Q, K, V)}_{\text{text cross-attn}} + \lambda \cdot \underbrace{\text{Attention}(Q, K_b, V_b)}_{\text{bokeh cross-attn}}.$$
(10)

Empirically, attaching our adapter to the deeper cross-attention layers sufficiently shapes the final texture while minimizing leakage. Fig. 6 illustrates how text and bokeh features are combined for defocus control without disrupting scene semantics. In addition, we adapt the attention localization strategy from Xiao et al. [2023] to steer bokeh attention to the background region during training.

Imposing Scene-consistent Bokeh Generation

Grounded self-attention. While bokeh cross-attention effectively controls defocus blur for a single image, we observe unwanted content shifts when applying different blur levels to the same scene (i.e., same text prompt and random seed). To address this, we introduce our grounded self-attention mechanism (see Fig. 6). We designate a random *pivot* image in each contrastive batch as a structural anchor for the other images during training: the pivot's queries enforce a consistent scene layout, while the keys are concatenated from both pivot and target images to align each defocus level with the pivot's content. Exposing the model to such paired examples teaches it to disentangle bokeh intensity from scene contents.

Formally, let Q_{tgt} , K_{tgt} , V_{tgt} be the query, key, and value projections from the deep features $h_{\rm tgt}$ of image $I_{\rm tgt}$, and let $Q_{\rm piv}, K_{\rm piv}, V_{\rm piv}$ be those corresponding to a *pivot* image I_{piv} . We replace the usual self-attention with:

Attention(
$$Q_{piv}$$
, [K_{tgt} , K_{piv}], [V_{tgt} , V_{tgt}]), (11)

where $[\cdot,\cdot]$ indicates concatenation, and h_{piv} retains its standard self-attention. In other words, the pivot's query Q_{piv} anchors the structural layout, while concatenating K_{tgt} and K_{piv} helps the model learn correspondences between I_{tgt} and I_{piv} . Since the values come from V_{tgt} (duplicated), the resulting denoised features inherit the defocus level of *I*_{tgt} while aligning with the pivot's scene.

To enable this cross-image guidance, we match the noise and timesteps for I_{tgt} and I_{piv} during training, so both images undergo synchronized diffusion. Consequently, the backward (denoising) process for I_{tgt} can be expressed as:

$$z_{t-1} \leftarrow \varepsilon_{\theta}(z_t, c, c_b, t; \{Q_{\text{piv}}^t, K_{\text{piv}}^t\}),$$
 (12)

where z_{t-1} denotes the predicted latent at timestep (t-1), c is the textual context, c_b the bokeh condition, and $\{Q_{\text{piv}}^t, K_{\text{piv}}^t\}$ are the pivot's queries and keys at timestep t.

3.4.2 Color transfer. Although our model mitigates most inconsistencies, we observe occasional biases in lighting or color between different defocus levels. To address this, we apply a post-processing step that aligns the color distribution of the target bokeh image with the pivot. This phenomenon has also been reported in related diffusion model applications [Yang et al. 2023], where it is commonly addressed using AdaIN [Huang and Belongie 2017] in the latent space. Instead, inspired by the classic color-transfer method of Reinhard et al. [2001], we operate in the $L^*a^*b^*$ color space (a visual comparison with AdaIN is provided in the supplementary material). We update each channel C of image I_{tgt} as:

$$I_{\text{tgt}} \leftarrow \frac{\sigma_{\text{piv}}}{\sigma_{\text{tot}}} \left(I_{\text{tgt}} - \mu_{\text{tgt}} \right) + \mu_{\text{piv}},$$
 (13)

thus matching channel-wise first- and second-order statistics. This preserves perceptual sharpness relationships yet harmonizes lighting and color across the image pair.

Bokeh Diffusion in MMDiT Architecture

Recent state-of-the-art T2I models (e.g., FLUX [Labs 2024]) replace the traditional UNet-based denoising network with a Multimodal Diffusion Transformer (MMDiT) [Esser et al. 2024]. In FLUX, the MMDiT backbone performs joint self-attention over concatenated text and image tokens within a single, unified operation:

Attention
$$([Q_{\text{txt}}, \text{RoPE}(Q_{\text{img}})], [K_{\text{txt}}, \text{RoPE}(K_{\text{img}})], [V_{\text{txt}}, V_{\text{img}}])$$
 (14)

where Rotary Positional Embedding (RoPE) [Su et al. 2024] is injected only into image queries and keys, while text tokens keep all-zero positional encoding.

Since MMDiT no longer separates self- from cross-attention, we insert both bokeh conditioning and pivot-based grounding directly into its joint attention module. Let $Q_{\text{piv}} = [Q_{\text{txt}}^{\text{piv}}, \text{RoPE}(Q_{\text{imo}}^{\text{piv}})]$

Table 1. Quantitative comparison against pretrained and finetuned baselines. *Accuracy* is measured by the Laplacian variance trend correlation to the reference (LVCorr) and GPT-40 estimations. *Consistency* is measured by LPIPS (closer to reference is better) and GPT-40 scores. *Quality* is evaluated using ImageReward (IR). The best result is showcased in **bold**, and the second-best underlined.

Type	Method	Accuracy	(CorrCoef)	Consistency		Quality
1) pc	Method	LVCorr ↑	GPT-4o↑	LPIPS	GPT-4o↑	IR↑
Reference	BokehMe [Peng et al. 2022]	1.000	0.941	0.075	96.65	_
Pretrained	SD1.5 [Rombach et al. 2022] FLUX [Labs 2024]	-0.206 -0.033	0.362 0.336	0.314 0.177	68.75 78.25	1.065 1.280
Finetuned	CSaT [Fang et al. 2024] CSaT + ControlNet [Fang et al. 2024] GenPhoto [Yuan et al. 2024] Bokeh Diffusion (SD1.5) Bokeh Diffusion (FLUX)	-0.044 0.498 0.796 <u>0.904</u> 0.917	0.628 0.784 0.826 0.960 0.985	0.155 0.178 0.197 0.080 <u>0.052</u>	73.00 67.25 86.50 <u>94.75</u> 98.16	0.509 0.335 -1.471 0.988 <u>1.093</u>

Table 2. User preference rates.

	CSaT	CSaT+CN	GenPhoto	Ours
Bokeh Control	4.00%	2.67%	2.33%	91.00%
Scene Consistency	2.33%	2.33%	2.67%	92.67%
Text-Image Align.	13.00%	10.00%	3.00%	74.00%

denote the concatenated pivot queries, and define K_{tgt} , K_{piv} , V_{tgt} analogously, the Bokeh Diffusion attention modules from Sec. 3.3 and Sec. 3.4 are jointly defined in FLUX as:

Attention(
$$Q_{\text{piv}}$$
, [K_{tgt} , K_{piv}], [V_{tgt} , V_{tgt}])
+ λ Attention(Q_{piv} , K_b , V_b). (15)

This adaptation makes our framework fully compatible with FLUX.

4 EXPERIMENTS

4.1 Scene-consistent Defocus Blur Control

4.1.1 Comparison with baselines. We compare our method against two pretrained text-to-image (T2I) diffusion models, SD1.5 [Rombach et al. 2022] and FLUX [Labs 2024], as well as two related methods that finetune diffusion models for photographic controls, Camera Settings as Tokens (CSaT) [Fang et al. 2024] and Generative Photography (GenPhoto) [Yuan et al. 2024]. As a reference, we also include blur renderings from BokehMe [Peng et al. 2022].

Quantitative evaluation. We benchmark on 20 diverse prompts, each with 5 different bokeh conditions, totaling 100 samples. The quantitative evaluation focuses on three aspects:

- Accuracy: We measure how each method's bokeh aligns with
 the target blur parameter via CorrCoef [Yuan et al. 2024].
 Specifically, we compute the Laplacian variance trend for
 images in a scene under different blur conditions and obtain
 the Pearson correlation with the reference trend (LVCorr).
 A higher correlation indicates more faithful defocus control.
 Additionally, we employ GPT-4o [OpenAI 2024] to estimate
 the bokeh level of a batch of images and calculate the Pearson
 correlation with its conditioning sequence.
- Consistency: We examine whether the blur level causes unintended shifts in the scene. We use LPIPS [Zhang et al. 2018] to quantify how distant images with same prompt but different blur conditions are. It is important to note that lower is

not always better, since the change in depth-of-field should affect perceptual distance to some extent. We consider best the closest result to the reference. Additionally, we employ GPT-40 [OpenAI 2024] to rate how consistent a batch of images remain despite depth-of-field variations.

• *Quality*: We use ImageReward [Xu et al. 2023], a general-purpose T2I preference reward model, to assess the perceptual quality and prompt alignment of generated images.

Table 1 shows that our approach outperforms all baselines by a significant margin. Pretrained T2I diffusion models struggle to achieve reliable control over depth-of-field, as reflected in their low accuracy scores. Furthermore, modifying the condition frequently alters the scene, as evidenced by the consistency scores. While recent finetuned methods improve upon the pretrained backbones in those two dimensions, they still fall short of our results. In terms of generation quality, our method achieves scores comparable to its respective pretrained backbone, indicating that our framework introduces scene-consistent bokeh control while largely maintaining the original generation quality. Compared to GenPhoto, which operates within a T2V framework and relies on batched generation with several frames, our method is built entirely within the T2I paradigm, allowing our model to be integrated into state-of-the-art T2I systems, inheriting their generation quality.

Qualitative evaluation. As shown in Fig. 8, CSaT often alters the scene layout when changing bokeh levels, due to entangled conditioning. Even when combined with ControlNet [Zhang et al. 2023], as proposed by the authors, consistency is only coarse and the underlying content can still vary significantly. This inconsistency also affects the intended defocus effect, as the perception of bokeh depends on consistent subject-background relationships. GenPhoto improves scene stability by operating in the T2V domain with batched inference. However, its results at low bokeh levels often look overly textured or flat (e.g., lantern and painting scenes). It also exhibits subtle inconsistencies in content preservation, particularly in fine details and color distribution (e.g., clay pot and painting cases). In contrast, our method generates the full range of bokeh levels accurately and with high perceptual quality, while maintaining strong scene and content consistency.

Table 3.	Quantitative	ablation	study on	SD1.5	version.
----------	--------------	----------	----------	-------	----------

Method	Dataset		Accuracy		Consistency	
Wictiou	ITW	SYN	LVCorr	GPT-40	LPIPS	GPT-40
Reference	-	-	1.000	0.941	0.075	96.65
Pretrained SD1.5	-	-	-0.206	0.362	0.314	68.75
+ Bokeh Cross-Attn	✓ × ✓	X ✓	0.705 0.698 0.722	0.304 0.618 0.690	0.098 0.202 0.171	90.50 80.00 80.00
+ Grounded Self-Attn + Color Transfer	√	√	0.902 0.904	0.943 0.960	0.089 0.080	94.00 94.75

User study. Table 2 summarizes the results of a user study conducted with 20 participants. Each participant was shown 15 generated scenes, where outputs from different methods were presented as short sequences of images depicting increasing bokeh levels. The method order was shuffled per scene to ensure anonymity. For each sequence, users were asked to select the method they preferred along three dimensions: (1) the effectiveness of bokeh control; (2) scene consistency; and (3) text-image alignment. This study serves as another key evaluation metric. Across all dimensions, participants showed a clear preference for our method.

4.1.2 Image editing. Our framework accommodates two usage scenarios: (i) Unbounded bokeh generation, where a user can directly sample an image at the desired blur level using the conventional self-attention mechanism. (ii) Grounded bokeh generation, where a pivot image is chosen to anchor the scene whose bokeh the user wants to adjust. Since we randomly pick a pivot in each contrastive batch during training, the grounded self-attention module in our model learns to either add or remove blur relative to that pivot. Consequently, at inference time we can choose any pivot image with a given bokeh level and request a new target level. Fig. 10 demonstrates how using either a sharper or blurrier pivot yields results matching the requested bokeh parameter without changing its contents. Additionally, we also support editing real images by first inverting them via a diffusion inversion procedure [Song et al. 2020], then simultaneously denoising two latents: one to reconstruct the original image (used as pivot) and one to apply a new bokeh setting. Fig. 11 shows how our approach can natively add or reduce blur in a real image with minimal artifacts through inversion.

Ablation Study

We investigate two main aspects of our pipeline: training data composition and the method for imposing consistency.

4.2.1 Training data. We train on three different settings: (i) only in-the-wild (ITW) data, (ii) only synthetic (SYN) blur augmentations, and (iii) a dataset combining both. Table 3 shows the mixed setting achieves the best overall accuracy while also improving consistency compared to training solely on SYN data. Training on ITW data alone results in high consistency but lower accuracy. We hypothesize that the diversity and potential noise in real image annotations make it hard for the model to learn a clear correlation between the conditioning signal and the bokeh effect. As a result, the model learns to apply only a limited bokeh range. Conversely, training



Fig. 7. Ablation of the proposed modules of Bokeh Diffusion.

exclusively on SYN data allows for fast convergence but degrades the generation quality and generalization ability of the model.

4.2.2 Imposing scene consistency. We ablate key components of our method to understand their contribution to achieving sceneconsistent bokeh control. Starting with the bokeh cross-attention module alone, we observe improved defocus control, indicating that explicitly conditioning on a physical blur parameter already enables the model to modulate depth-of-field meaningfully. However, without additional structure guidance, content shifts occur across different blur levels. Adding grounded self-attention significantly enhances scene consistency, ensuring that spatial layout remains aligned as the blur strength varies. This validates our design of using pivot-based guidance to anchor the structure of the generated image. Lastly, while the color transfer step is optional, it further improves visual coherence by harmonizing lighting and tone, without interfering with the defocus itself. Fig. 7 provides a visual example of the contribution of each component.

LIMITATIONS AND DISCUSSION

Fig. 12 illustrates a few representative failure cases of our method, reflecting data-driven tendencies. Our approach relies on in-the-wild images enriched with inferred parameters (including metric depth and a heuristic focus distance), which inevitably introduces approximation error. Beyond this, some observed failures appear rooted in common photographic conventions (Fig. 12a, Fig. 12b). Additionally, since most training scenes contain a clear foreground subject, the model may over-assume such structure and hallucinate foreground content when none exists (Fig. 12c). These observations motivate promising future extensions. A key direction is enabling flexible focal-plane control, allowing the sharp region to slide through the scene. We also envision conditioning on other photographic settings (e.g., exposure) and extending our method to image-to-image diffusion for improved real-image editing use cases.

6 CONCLUSION

In this work, we introduced Bokeh Diffusion, a text-to-image framework that enables precise defocus blur control while maintaining scene consistency. We integrate in-the-wild images with synthetic blur augmentations to balance realism and robustness, while our grounded self-attention mechanism enforces structural consistency across blur levels. Experiments show our method surpasses baselines in both accuracy and scene consistency, offering flexible, lens-like bokeh adjustments. We hope this work inspires further research into fine-grained photographic controls in generative models.

REFERENCES

- Abdullah Abuolaim and Michael S Brown. 2020. Defocus Deblurring Using Dual-Pixel Data. In European Conference on Computer Vision. Springer, 111–126.
- Yuval Alaluf, Daniel Garibi, Or Patashnik, Hadar Averbuch-Elor, and Daniel Cohen-Or. 2024. Cross-Image Attention for Zero-Shot Appearance Transfer. In ACM SIGGRAPH 2024 Conference Papers (SIGGRAPH '24). Association for Computing Machinery, New York, NY, USA, 1–12. https://doi.org/10.1145/3641519.3657423
- Fan Bao, Shen Nie, Kaiwen Xue, Yue Cao, Chongxuan Li, Hang Su, and Jun Zhu. 2023a. All Are Worth Words: A ViT Backbone for Diffusion Models. In 2023 IEEE/CVF Conference on Computer Vision and Pattern Recognition (CVPR). 22669–22679. https://doi.org/10.1109/CVPR52729.2023.02171
- Fan Bao, Shen Nie, Kaiwen Xue, Chongxuan Li, Shi Pu, Yaole Wang, Gang Yue, Yue Cao, Hang Su, and Jun Zhu. 2023b. One Transformer Fits All Distributions in Multi-Modal Diffusion at Scale. In Proceedings of the 40th International Conference on Machine Learning. PMLR, 1692–1717. https://proceedings.mlr.press/v202/bao23a.html
- Aleksei Bochkovskii, Amaël Delaunoy, Hugo Germain, Marcel Santos, Yichao Zhou, Stephan R. Richter, and Vladlen Koltun. 2024. Depth Pro: Sharp Monocular Metric Depth in Less Than a Second. https://doi.org/10.48550/arXiv.2410.02073 arXiv:2410.02073 [cs]
- Mingdeng Cao, Xintao Wang, Zhongang Qi, Ying Shan, Xiaohu Qie, and Yinqiang Zheng. 2023. MasaCtrl: Tuning-Free Mutual Self-Attention Control for Consistent Image Synthesis and Editing. In Proceedings of the IEEE/CVF International Conference on Computer Vision (ICCV). 22560–22570.
- Junsong Chen, Chongjian Ge, Enze Xie, Yue Wu, Lewei Yao, Xiaozhe Ren, Zhongdao Wang, Ping Luo, Huchuan Lu, and Zhenguo Li. 2024a. PixArt-\$\Sigma\$: Weak-to-Strong Training of Diffusion Transformer for 4K Text-to-Image Generation. https://doi.org/10.48550/arXiv.2403.04692 arXiv:2403.04692 [cs]
- Junsong Chen, Jincheng Yu, Chongjian Ge, Lewei Yao, Enze Xie, Zhongdao Wang, James Kwok, Ping Luo, Huchuan Lu, and Zhenguo Li. 2023. PixArt-\$\alpha\\$: Fast Training of Diffusion Transformer for Photorealistic Text-to-Image Synthesis. In The Twelfth International Conference on Learning Representations. https://openreview.net/forum?id=eAKmQPe3m1
- Lin Chen, Jinsong Li, Xiaoyi Dong, Pan Zhang, Conghui He, Jiaqi Wang, Feng Zhao, and Dahua Lin. 2024b. Sharegpt4v: Improving Large Multi-Modal Models with Better Captions. In European Conference on Computer Vision. Springer, 370–387.
- Zhe Chen, Jiannan Wu, Wenhai Wang, Weijie Su, Guo Chen, Sen Xing, Muyan Zhong, Qinglong Zhang, Xizhou Zhu, Lewei Lu, et al. 2024c. Internvl: Scaling up Vision Foundation Models and Aligning for Generic Visual-Linguistic Tasks. In Proceedings of the IEEE/CVF Conference on Computer Vision and Pattern Recognition. 24185–24198.
- Ta-Ying Cheng, Matheus Gadelha, Thibault Groueix, Matthew Fisher, Radomir Mech, Andrew Markham, and Niki Trigoni. 2024. Learning Continuous 3D Words for Text-to-Image Generation. arXiv preprint arXiv:2402.08654 (2024). arXiv:2402.08654
- Patrick Esser, Sumith Kulal, Andreas Blattmann, Rahim Entezari, Jonas Müller, Harry Saini, Yam Levi, Dominik Lorenz, Axel Sauer, Frederic Boesel, Dustin Podell, Tim Dockhorn, Zion English, and Robin Rombach. 2024. Scaling Rectified Flow Transformers for High-Resolution Image Synthesis. In Forty-First International Conference on Machine Learning. https://openreview.net/forum?id=FPnUhsQJ5B
- I-Sheng Fang, Yue-Hua Han, and Jun-Cheng Chen. 2024. Camera Settings as Tokens: Modeling Photography on Latent Diffusion Models. In SIGGRAPH Asia 2024 Conference Papers (SA '24). Association for Computing Machinery, New York, NY, USA,

- 1-11. https://doi.org/10.1145/3680528.3687635
- Michael Freeman. 2007. The Photographer's Eye: Composition and Design for Better Digital Photos (1 ed.). Focal Press, Burlington, MA.
- Nicholas Guttenberg. 2023. Diffusion with Offset Noise. https://www.crosslabs.org/blog/diffusion-with-offset-noise
- Tiankai Hang, Shuyang Gu, Chen Li, Jianmin Bao, Dong Chen, Han Hu, Xin Geng, and Baining Guo. 2023. Efficient Diffusion Training via Min-SNR Weighting Strategy. In Proceedings of the IEEE/CVF International Conference on Computer Vision 7441–7451. https://openaccess.thecvf.com/content/ICCV2023/html/Hang_Efficient_Diffusion_Training_via_Min-SNR_Weighting_Strategy_ICCV_2023_paper.html
- Hao He, Yinghao Xu, Yuwei Guo, Gordon Wetzstein, Bo Dai, Hongsheng Li, and Ceyuan Yang. 2024. CameraCtrl: Enabling Camera Control for Text-to-Video Generation.
- Amir Hertz, Ron Mokady, Jay Tenenbaum, Kfir Aberman, Yael Pritch, and Daniel Cohenor. 2022. Prompt-to-Prompt Image Editing with Cross-Attention Control. In *The Eleventh International Conference on Learning Representations*. https://openreview.net/forum?id= CDixzkzeyb
- Amir Hertz, Andrey Voynov, Shlomi Fruchter, and Daniel Cohen-Or. 2024. Style Aligned Image Generation via Shared Attention. In 2024 IEEE/CVF Conference on Computer Vision and Pattern Recognition (CVPR). 4775–4785. https://doi.org/10.1109/CVPR52733.2024.00457
- Jonathan Ho, Ajay Jain, and Pieter Abbeel. 2020. Denoising Diffusion Probabilistic Models. In Advances in Neural Information Processing Systems, Vol. 33. Curran Associates, Inc., 6840–6851. https://proceedings.neurips.cc/paper/2020/hash/4c5bcfec8584af0d967f1ab10179ca4b-Abstract.html
- Lukas Höllein, Aljaž Božič, Norman Müller, David Novotny, Hung-Yu Tseng, Christian Richardt, Michael Zollhöfer, and Matthias Nießner. 2024. ViewDiff: 3D-Consistent Image Generation with Text-To-Image Models. In Proceedings of the IEEE/CVF Conference on Computer Vision and Pattern Recognition.
- Edward J Hu, Yelong Shen, Phillip Wallis, Zeyuan Allen-Zhu, Yuanzhi Li, Shean Wang, Lu Wang, Weizhu Chen, et al. 2022. Lora: Low-rank Adaptation of Large Language Models. ICLR 1. 2 (2022). 3.
- Xun Huang and Serge Belongie. 2017. Arbitrary Style Transfer in Real-Time With Adaptive Instance Normalization. In *Proceedings of the IEEE International Conference on Computer Vision*. 1501–1510. https://openaccess.thecvf.com/content_iccv_2017/html/Huang_Arbitrary_Style_Transfer_ICCV_2017_paper.html
- Andrey Ignatov, Jagruti Patel, and Radu Timofte. 2020. Rendering Natural Camera Bokeh Effect with Deep Learning. In Proceedings of the IEEE/CVF Conference on Computer Vision and Pattern Recognition Workshops. 418–419.
- Tero Karras, Miika Aittala, Timo Aila, and Samuli Laine. 2022. Elucidating the Design Space of Diffusion-Based Generative Models. In Advances in Neural Information Processing Systems, S. Koyejo, S. Mohamed, A. Agarwal, D. Belgrave, K. Cho, and A. Oh (Eds.), Vol. 35. Curran Associates, Inc., 26565–26577. https://proceedings.neurips.cc/paper_files/paper/2022/file/a98846e9d9cc01cfb87eb694d946ce6b-Paper-Conference.pdf
- Nupur Kumari, Grace Su, Richard Zhang, Taesung Park, Eli Shechtman, and Jun-Yan Zhu. 2024. Customizing Text-to-Image Diffusion with Object Viewpoint Control. In SIGGRAPH Asia.
- Black Forest Labs. 2024. FLUX. https://github.com/black-forest-labs/flux
- Reginald L. Lagendijk and Jan Biemond. 2009. Chapter 14 Basic Methods for Image Restoration and Identification. In *The Essential Guide to Image Processing*, Al Bovik (Ed.). Academic Press, Boston, 323–348. https://doi.org/10.1016/B978-0-12-374457-9.00014-7
- Michael Langford, Anna Fox, and Richard Sawdon Smith. 2015. *Langford's Basic Photography: The Guide for Serious Photographers* (10 ed.). Focal Press, Taylor & Francis Group, Abingdon, UK.
- Yaron Lipman, Ricky T. Q. Chen, Heli Ben-Hamu, Maximilian Nickel, and Matthew Le. 2022. Flow Matching for Generative Modeling. In The Eleventh International Conference on Learning Representations. https://openreview.net/forum?id=PqvMRDCJT9t
- Xingchao Liu, Chengyue Gong, and Qiang Liu. 2022. Flow Straight and Fast: Learning to Generate and Transfer Data with Rectified Flow. In The Eleventh International Conference on Learning Representations. https://openreview.net/forum?id=XVjTT1nw5z
- Ilya Loshchilov and Frank Hutter. 2018. Decoupled Weight Decay Regularization. In International Conference on Learning Representations. https://openreview.net/forum?id=Bkg6RiCgV7
- Cheng Lu, Yuhao Zhou, Fan Bao, Jianfei Chen, Chongxuan LI, and Jun Zhu. 2022. DPM-Solver: A Fast ODE Solver for Diffusion Probabilistic Model Sampling in Around 10 Steps. In Advances in Neural Information Processing Systems, S. Koyejo, S. Mohamed, A. Agarwal, D. Belgrave, K. Cho, and A. Oh (Eds.), Vol. 35. Curran Associates, Inc., 5775–5787. https://proceedings.neurips.cc/paper_files/paper/2022/file/260a14acce2a89dad36adc8eefe7c59e-Paper-Conference.pdf
- Konstantin Mishchenko and Aaron Defazio. 2024. Prodigy: An Expeditiously Adaptive Parameter-Free Learner. https://doi.org/10.48550/arXiv.2306.06101 arXiv:2306.06101 [cs]
- Chong Mou, Xintao Wang, Liangbin Xie, Yanze Wu, Jian Zhang, Zhongang Qi, Ying Shan, and Xiaohu Qie. 2023. T2I-Adapter: Learning Adapters to Dig out More Controllable Ability for Text-to-Image Diffusion Models. https://doi.org/10.48550/

- arXiv.2302.08453 arXiv:2302.08453 [cs]
- Alexander Quinn Nichol, Prafulla Dhariwal, Aditya Ramesh, Pranav Shyam, Pamela Mishkin, Bob Mcgrew, Ilya Sutskever, and Mark Chen. 2022. GLIDE: Towards Photorealistic Image Generation and Editing with Text-Guided Diffusion Models. In Proceedings of the 39th International Conference on Machine Learning. PMLR, 16784-16804. https://proceedings.mlr.press/v162/nichol22a.html
- NVIDIA, Yuval Atzmon, Maciej Bala, Yogesh Balaji, Tiffany Cai, Yin Cui, Jiaojiao Fan, Yunhao Ge, Siddharth Gururani, Jacob Huffman, Ronald Isaac, Pooya Jannaty, Tero Karras, Grace Lam, J. P. Lewis, Aaron Licata, Yen-Chen Lin, Ming-Yu Liu, Qianli Ma, Arun Mallya, Ashlee Martino-Tarr, Doug Mendez, Seungjun Nah, Chris Pruett, Fitsum Reda, Jiaming Song, Ting-Chun Wang, Fangyin Wei, Xiaohui Zeng, Yu Zeng, and Qinsheng Zhang. 2024. Edify Image: High-Quality Image Generation with Pixel Space Laplacian Diffusion Models. https://doi.org/10.48550/arXiv.2411.07126 arXiv:2411.07126 [cs]
- OpenAI. 2024. GPT-4o System Card. arXiv preprint arXiv:2410.21276 (2024). arXiv:2410.21276 https://arxiv.org/abs/2410.21276
- William Peebles and Saining Xie. 2023. Scalable Diffusion Models with Transformers. In 2023 IEEE/CVF International Conference on Computer Vision (ICCV). IEEE Computer Society, Los Alamitos, CA, USA, 4172-4182. https://doi.org/10.1109/ICCV51070.
- Juewen Peng, Zhiguo Cao, Xianrui Luo, Hao Lu, Ke Xian, and Jianming Zhang. 2022. BokehMe: When Neural Rendering Meets Classical Rendering. In 2022 IEEE/CVF Conference on Computer Vision and Pattern Recognition (CVPR). IEEE, New Orleans, LA, USA, 16262-16271. https://doi.org/10.1109/cvpr52688.2022.01580
- Juewen Peng, Xianrui Luo, Ke Xian, and Zhiguo Cao. 2021. Interactive Portrait Bokeh Rendering System. In 2021 IEEE International Conference on Image Processing (ICIP). 2923-2927. https://doi.org/10.1109/ICIP42928.2021.9506674
- Dustin Podell, Zion English, Kyle Lacey, Andreas Blattmann, Tim Dockhorn, Jonas Müller, Joe Penna, and Robin Rombach. 2023. SDXL: Improving Latent Diffusion Models for High-Resolution Image Synthesis. https://doi.org/10.48550/arXiv.2307. 01952 arXiv:2307.01952 [cs]
- E. Reinhard, M. Adhikhmin, B. Gooch, and P. Shirley. 2001. Color Transfer between Images. IEEE Computer Graphics and Applications 21, 5 (July 2001), 34-41. https:// //doi.org/10.1109/38.946629
- Robin Rombach, Andreas Blattmann, Dominik Lorenz, Patrick Esser, and Björn Ommer. 2022. High-Resolution Image Synthesis With Latent Diffusion Models. In ${\it Proceedings}$ of the IEEE/CVF Conference on Computer Vision and Pattern Recognition (CVPR). 10684-10695
- Nataniel Ruiz, Yuanzhen Li, Varun Jampani, Yael Pritch, Michael Rubinstein, and Kfir Aberman. 2023. DreamBooth: Fine Tuning Text-to-Image Diffusion Models for Subject-Driven Generation. In 2023 IEEE/CVF Conference on Computer Vision and Pattern Recognition (CVPR). 22500-22510. https://doi.org/10.1109/CVPR52729.2023. 02155
- Chitwan Saharia, William Chan, Saurabh Saxena, Lala Lit, Jay Whang, Emily Denton, Seyed Kamyar Seyed Ghasemipour, Burcu Karagol Ayan, S. Sara Mahdavi, Raphael Gontijo-Lopes, Tim Salimans, Jonathan Ho, David J Fleet, and Mohammad Norouzi. 2022. Photorealistic Text-to-Image Diffusion Models with Deep Language Understanding. In Proceedings of the 36th International Conference on Neural Information Processing Systems (NIPS '22). Curran Associates Inc., Red Hook, NY, USA, 36479-36494
- Yichen Sheng, Zixun Yu, Lu Ling, Zhiwen Cao, Xuaner Zhang, Xin Lu, Ke Xian, Haiting Lin, and Bedrich Benes. 2024. Dr. Bokeh: DiffeRentiable Occlusion-aware Bokeh Rendering. In Proceedings of the IEEE/CVF Conference on Computer Vision and Pattern Recognition. 4515-4525. https://openaccess.thecvf.com/content/CVPR2024/html/Sheng_Dr._Bokeh DiffeRentiable_Occlusion-aware_Bokeh_Rendering_CVPR_2024_paper.html
- Jascha Sohl-Dickstein, Eric Weiss, Niru Maheswaranathan, and Surya Ganguli. 2015. Deep Unsupervised Learning Using Nonequilibrium Thermodynamics. In Proceedings of the 32nd International Conference on Machine Learning. PMLR, 2256-2265. https://proceedings.mlr.press/v37/sohl-dickstein15.html
- Jiaming Song, Chenlin Meng, and Stefano Ermon. 2020. Denoising Diffusion Implicit Models. In International Conference on Learning Representations. https://openreview. net/forum?id=St1giarCHLP
- Jianlin Su, Murtadha Ahmed, Yu Lu, Shengfeng Pan, Wen Bo, and Yunfeng Liu. 2024. Roformer: Enhanced Transformer with Rotary Position Embedding. Neurocomputing
- Wenqiang Sun, Shuo Chen, Fangfu Liu, Zilong Chen, Yueqi Duan, Jun Zhang, and Yikai Wang. 2024. DimensionX: Create Any 3D and 4D Scenes from a Single Image with Controllable Video Diffusion. arXiv preprint arXiv:2411.04928 (2024). arXiv:2411.04928
- Andrey Voynov, Amir Hertz, Moab Arar, Shlomi Fruchter, and Daniel Cohen-Or. 2024. Curved Diffusion: A Generative Model with Optical Geometry Control. In Computer Vision - ECCV 2024. Springer Nature Switzerland, 149-164.
- Neal Wadhwa, Rahul Garg, David E. Jacobs, Bryan E. Feldman, Nori Kanazawa, Robert Carroll, Yair Movshovitz-Attias, Jonathan T. Barron, Yael Pritch, and Marc Levoy. 2018. Synthetic Depth-of-Field with a Single-Camera Mobile Phone. ACM Trans.

- Graph. 37, 4 (July 2018), 64:1-64:13. https://doi.org/10.1145/3197517.3201329
- Chao Wang, Ana Serrano, Xingang Pan, Krzysztof Wolski, Bin Chen, Karol Myszkowski, Hans-Peter Seidel, Christian Theobalt, and Thomas Leimkühler. 2023a. An Implicit Neural Representation for the Image Stack: Depth, All in Focus, and High Dynamic Range. ACM Transactions on Graphics 42, 6 (Dec. 2023), 1-11. https://doi.org/10.
- Haofan Wang, Matteo Spinelli, Qixun Wang, Xu Bai, Zekui Qin, and Anthony Chen. 2024b. InstantStyle: Free Lunch towards Style-Preserving in Text-to-Image Generation. https://doi.org/10.48550/arXiv.2404.02733 arXiv:2404.02733 [cs]
- Xiaojuan Wang, Janne Kontkanen, Brian Curless, Steven M. Seitz, Ira Kemelmacher-Shlizerman, Ben Mildenhall, Pratul Srinivasan, Dor Verbin, and Aleksander Holynski. 2024a. Generative Powers of Ten. In Proceedings of the IEEE/CVF Conference on Computer Vision and Pattern Recognition. 7173–7182. https://openaccess.thecvf.com/content/CVPR2024/html/Wang_Generative_ Powers_of_Ten_CVPR_2024_paper.html
- Zhouxia Wang, Ziyang Yuan, Xintao Wang, Yaowei Li, Tianshui Chen, Menghan Xia, Ping Luo, and Ying Shan. 2023b. MotionCtrl: A Unified and Flexible Motion Controller for Video Generation. ACM SIGGRAPH 2024 Conference Papers (2023).
- Bin Xiao, Haiping Wu, Weijian Xu, Xiyang Dai, Houdong Hu, Yumao Lu, Michael Zeng, Ce Liu, and Lu Yuan. 2024a. Florence-2: Advancing a Unified Representation for a Variety of Vision Tasks. In Proceedings of the IEEE/CVF Conference on Computer Vision and Pattern Recognition. 4818-4829.
- Guangxuan Xiao, Tianwei Yin, William T. Freeman, Frédo Durand, and Song Han. 2023. FastComposer: Tuning-Free Multi-Subject Image Generation with Localized Attention. https://doi.org/10.48550/arXiv.2305.10431 arXiv:2305.10431 [cs]
- Zeqi Xiao, Wenqi Ouyang, Yifan Zhou, Shuai Yang, Lei Yang, Jianlou Si, and Xingang Pan. 2025. Trajectory Attention for Fine-Grained Video Motion Control. In The $Thirteenth\ International\ Conference\ on\ Learning\ Representations.\ \ https://openreview.$ net/forum?id=2z1HT5lw5M
- Zeqi Xiao, Yifan Zhou, Shuai Yang, and Xingang Pan. 2024b. Video Diffusion Models Are Training-free Motion Interpreter and Controller. In The Thirty-eighth Annual $Conference\ on\ Neural\ Information\ Processing\ Systems.\ \ https://openreview.net/forum?$ id=ZvO4Bn75kN
- Jiazheng Xu, Xiao Liu, Yuchen Wu, Yuxuan Tong, Qinkai Li, Ming Ding, Jie Tang, and Yuxiao Dong. 2023. ImageReward: Learning and Evaluating Human Preferences for Text-to-Image Generation. In Advances in Neural Information Processing Systems, A. Oh, T. Naumann, A. Globerson, K. Saenko, M. Hardt, and S. Levine (Eds.), Vol. 36. Curran Associates, Inc., 15903-15935. https://proceedings.neurips.cc/paper_files/ paper/2023/file/33646ef0ed554145eab65f6250fab0c9-Paper-Conference.pdf
- Shuai Yang, Yifan Zhou, Ziwei Liu, and Chen Change Loy. 2023. Rerender A Video: Zero-Shot Text-Guided Video-to-Video Translation. In SIGGRAPH Asia 2023 Conference Papers (SA '23). Association for Computing Machinery, New York, NY, USA, 1–11. https://doi.org/10.1145/3610548.3618160
- Yang Yang, Haiting Lin, Zhan Yu, Sylvain Paris, Jingyi Yu, Haiting Lin, Zhan Yu, Sylvain Paris, and Jingyi Yu. 2016. Virtual DSLR: High Quality Dynamic Depthof-Field Synthesis on Mobile Platforms. Electronic Imaging 28 (Feb. 2016), 1-9. https://doi.org/10.2352/ISSN.2470-1173.2016.18.DPMI-031
- Hu Ye, Jun Zhang, Sibo Liu, Xiao Han, and Wei Yang. 2023. IP-Adapter: Text Compatible Image Prompt Adapter for Text-to-Image Diffusion Models. https://doi.org/10. 48550/arXiv.2308.06721 arXiv:2308.06721 [cs]
- Yu Yuan, Xijun Wang, Yichen Sheng, Prateek Chennuri, Xingguang Zhang, and Stanley Chan. 2024. Generative Photography: Scene-Consistent Camera Control for Realistic Text-to-Image Synthesis. https://doi.org/10.48550/arXiv.2412.02168 arXiv:2412.02168 [cs]
- Lvmin Zhang, Anyi Rao, and Maneesh Agrawala. 2023. Adding Conditional Control to Text-to-Image Diffusion Models. In 2023 IEEE/CVF International Conference on Computer Vision (ICCV). 3813-3824. https://doi.org/10.1109/ICCV51070.2023.00355
- Richard Zhang, Phillip Isola, Alexei A. Efros, Eli Shechtman, and Oliver Wang. 2018. The Unreasonable Effectiveness of Deep Features as a Perceptual Metric. In 2018 IEEE/CVF Conference on Computer Vision and Pattern Recognition. 586-595. https: //doi.org/10.1109/CVPR.2018.00068
- Xuaner Zhang, Kevin Matzen, Vivien Nguyen, Dillon Yao, You Zhang, and Ren Ng. 2019. Synthetic Defocus and Look-Ahead Autofocus for Casual Videography. ACM Trans. Graph. 38, 4 (July 2019), 30:1-30:16. https://doi.org/10.1145/3306346.3323015
- Peng Zheng, Dehong Gao, Deng-Ping Fan, Li Liu, Jorma Laaksonen, Wanli Ouyang, and Nicu Sebe. 2024. Bilateral Reference for High-Resolution Dichotomous Image Segmentation. https://doi.org/10.48550/arXiv.2401.03407 arXiv:2401.03407 [cs]

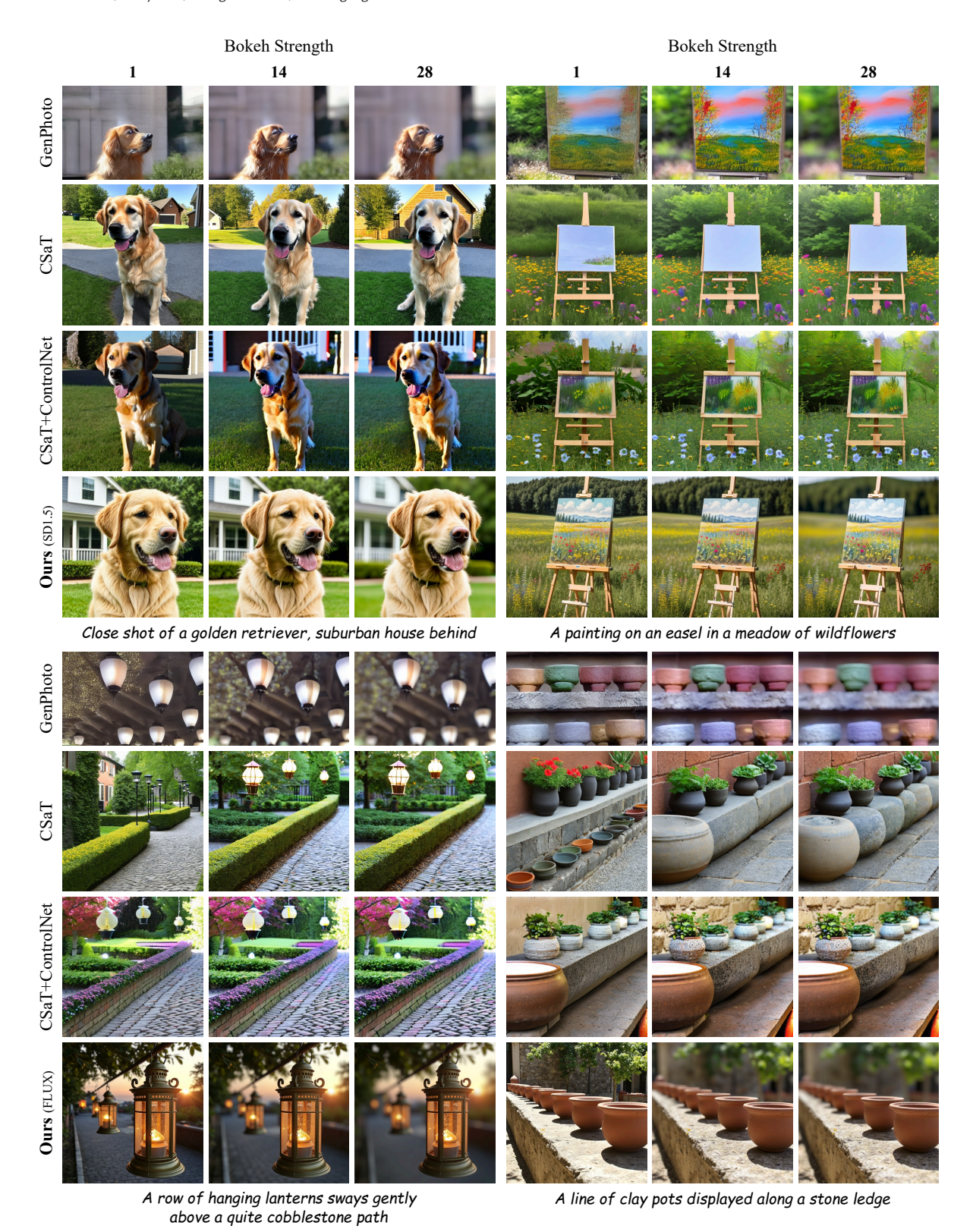


Fig. 8. Visual comparison with related generative models conditioned on photographic controls CSaT [Fang et al. 2024] and GenPhoto [Yuan et al. 2024].

More bokeh



Fig. 9. Additional comparison between our generative method and BokehMe [Peng et al. 2022], which depends on external depth estimation models.

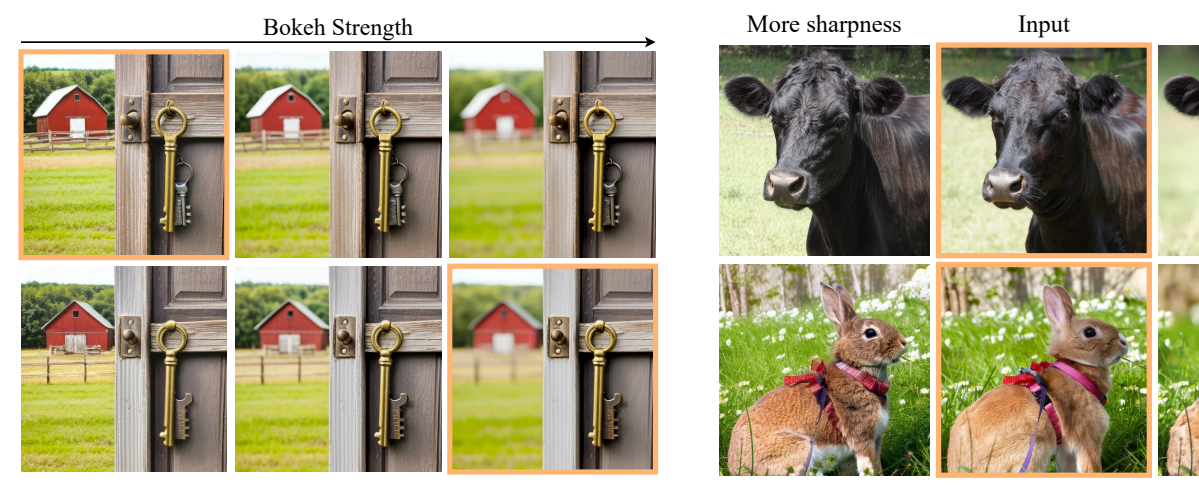


Fig. 10. Generated image editing with Bokeh Diffusion (SD1.5). By selecting a pivot image (highlighted in each row) with a given bokeh level, the model can increase or decrease defocus while maintaining scene composition.

Fig. 11. Real image editing with Bokeh Diffusion (SD1.5). A real photograph (highlighted) is inverted and denoised with a new bokeh condition, preserving structural details while modifying depth-of-field.



Fig. 12. Failure cases of our method. (a) Difficulty generating an all-in-focus image (left) in uncommon settings. Long-lens wildlife photos almost always exhibit strong background blur, such sharp examples are under-represented in training, so the model retains residual bokeh; (b) Over-sharpened foreground (right). (c) When no clear foreground is present (left), the model occasionally hallucinates spurious foreground elements if asked to increase bokeh (right).

Supplementary Material

A ADDITIONAL METHOD DETAILS

A.1 Dataset

A.1.1 Foreground reference and focus distance. Since EXIF data rarely includes an explicit focus distance S_1 , we approximate it by taking the median depth of the nearest portion of the foreground region. When the foreground depth range is small, we treat the entire foreground at a single S_1 to ensure a sharp subject.

A.1.2 Dataset alignment. Given the unified bokeh annotation K scale, Fig. 13 illustrates the alignment between the synthetic blur augmentations and the in-the-wild defocus patterns. The figure visually compares examples from both data sources, demonstrating that the synthetic approach closely replicates the depth-of-field characteristics observed in real photographs. This alignment validates our method for unifying the blur parameter K across diverse data, ensuring that the model learns consistent depth-of-field control.

A.1.3 Subject diversity. To further support our claim that existing multi-aperture datasets are limited in content diversity, Fig. 14 visualizes the distribution of scene content using wordclouds generated from vision-language model captions [Chen et al. 2024b]. Specifically, we compare the captions extracted from the DPDD dataset [Abuolaim and Brown 2020]—a prominent multi-aperture dataset—with those from our collected in-the-wild images. As seen in the visualization, DPDD predominantly features static, inanimate scenes such as indoor objects and tabletop arrangements. In contrast, our in-the-wild dataset spans a much broader range of subjects, including dynamic environments, natural scenes, and human-centered contexts. This diversity is crucial for training a generative model capable of realistic and generalizable bokeh control across varied prompts.

A.2 Localized cross-attention.

In addition to the decoupled cross-attention mechanism for bokeh condition injection, we adapt a localization strategy from Xiao et al. [2023] to steer the bokeh cross-attention toward the background region during training. Specifically, we downsample each foreground mask and measure the average bokeh cross-attention in the foreground and background. Analogously to Xiao et al. [2023], we then add a small regularization term that encourages higher attention values in the background and lower in the foreground. While this localization loss does not fully resolve scene inconsistency, it acts as a soft constraint that nudges the model toward learning more interpretable and spatially aware defocus behavior, providing mild supervision that complements the rest of the framework.

A.3 Algorithm

The pseudo-code for scene-consistent bokeh-conditioned sampling in the SD1.5 [Rombach et al. 2022] version of our method (UNetbased) is provided in Alg. 1. The FLUX [Labs 2024] version of our method is equivalent, aside from the fact that the decoupled bokeh cross-attention is perfomed in all layers and the number of default sampling and grounding steps is 30 and 18, respectively.

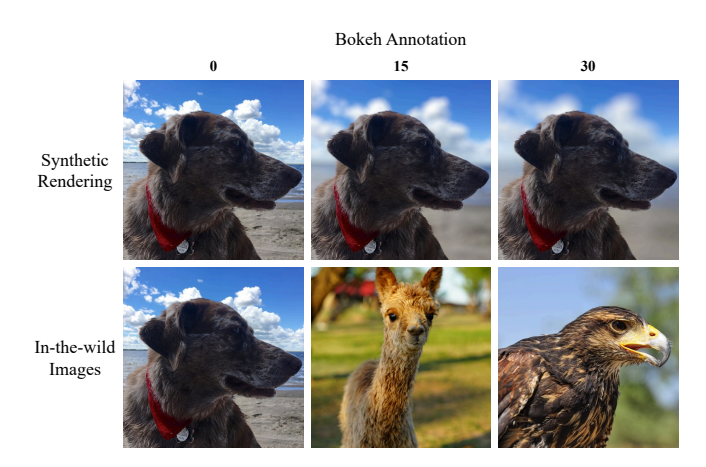


Fig. 13. Visualization of bokeh annotation alignment between collected inthe-wild images and synthetic bokeh augmentations using BokehMe [Peng et al. 2022] at 512×512 resolution.



Fig. 14. Wordclouds of captions extracted using a vision-language model for (a) DPDD [Abuolaim and Brown 2020] and (b) our in-the-wild dataset. Our dataset exhibits greater subject diversity, while the DPDD dataset focuses on static scenes with inanimate objects.

B ADDITIONAL EXPERIMENTAL DETAILS

B.1 Implementation Details

During training, each step samples either a real batch or a synthetic batch with equal probability (50%). In-the-wild batches use the conventional self-attention. In contrastive batches, we employ our grounded self-attention mechanism, where a single image in the batch is randomly selected as pivot for the others. Training data captions are taken from HuggingFace¹. For the SD1.5 [Rombach et al. 2022] version of our model, we use the AdamW optimizer [Loshchilov and Hutter 2018] with learning rate $1e^{-4}$ and total batch size 80. Following Guttenberg [2023], we apply a noise offset of 0.04. We also set a min-SNR of 2.0 [Hang et al. 2023]. We train for around 12K steps, taking approximately 3 hours on 4 NVIDIA RTX 4090 GPUs. At inference, we usually run 50 denoising steps

¹CaptionEmporium/flickr-megalith-10m-internvl2-multi-caption

Algorithm 1: Scene-Consistent Bokeh Sampling (SD1.5)

Input: Prompt \mathcal{P} ; pivot bokeh \mathcal{K}_{piv} ; target bokeh \mathcal{K}_{tgt} ; our finetuned T2I diffusion model ε_{θ} with L transformer blocks; decoder \mathcal{D} ; total sampling steps *T* (default 50); grounding cutoff *G* (default 30). **Output:** Image x^{tgt} matching \mathcal{K}_{tgt} while preserving the pivot scene of x^{piv} .

1 **Initialise** $z_T^{\text{piv}} \sim \mathcal{N}(0, 1), z_T^{\text{tgt}} \leftarrow z_T^{\text{piv}}$.

2 **for** t = T **to** T - G + 1 **do** for $\ell = 1$ to L do 3
$$\begin{split} & Q_{\mathrm{piv}}^{\ell}, K_{\mathrm{piv}}^{\ell}, V_{\mathrm{piv}}^{\ell} \leftarrow \varepsilon_{\theta}(z_{t}^{\mathrm{piv}}, t, \mathcal{P}, \mathcal{K}_{\mathrm{piv}}) \\ & Q_{\mathrm{tgt}}^{\ell}, K_{\mathrm{tgt}}^{\ell}, V_{\mathrm{tgt}}^{\ell} \leftarrow \varepsilon_{\theta}(z_{t}^{\mathrm{tgt}}, t, \mathcal{P}, \mathcal{K}_{\mathrm{tgt}}) \\ & A^{\ell} \leftarrow \mathrm{Attention}(Q_{\mathrm{piv}}^{\ell}, [K_{\mathrm{tgt}}^{\ell}, K_{\mathrm{piv}}^{\ell}], [V_{\mathrm{tgt}}^{\ell}, V_{\mathrm{tgt}}^{\ell}]) \end{split}$$
4 5 $\begin{aligned} & \textbf{if } \ell \in \mathcal{L}_{\text{deep}} \textbf{ then} \\ & \mid h^{\ell}_{\text{piv}} \leftarrow h^{\ell}_{\text{piv}} + \lambda \operatorname{Attention}(Q^{\ell}_{\text{piv}}, K^{\ell}_{b-\text{piv}}, V^{\ell}_{b-\text{piv}}) \\ & \mid h^{\ell}_{\text{tgt}} \leftarrow h^{\ell}_{\text{tgt}} + \lambda \operatorname{Attention}(Q^{\ell}_{\text{tgt}}, K^{\ell}_{b-\text{tgt}}, V^{\ell}_{b-\text{tgt}}) \end{aligned}$ 8 10 $z_{t-1}^{\text{piv}} \leftarrow \varepsilon_{\theta}(z_{t}^{\text{piv}}, t, \mathcal{P}, \mathcal{K}_{\text{piv}})$ $z_{t-1}^{\text{tgt}} \leftarrow \varepsilon_{\theta}(z_{t}^{\text{tgt}}, t, \mathcal{P}, \mathcal{K}_{\text{tgt}}, A)$ 15 **for** t = T - G **to** 1 **do**16 $z_{t-1}^{\text{piv}} \leftarrow \varepsilon_{\theta}(z_{t}^{\text{piv}}, t, \mathcal{P}, \mathcal{K}_{\text{piv}})$ 17 $z_{t-1}^{\text{tgt}} \leftarrow \varepsilon_{\theta}(z_{t}^{\text{tgt}}, t, \mathcal{P}, \mathcal{K}_{\text{tgt}})$ 19 $x^{\text{piv}} \leftarrow \mathcal{D}(z_0^{\text{piv}})$ 20 $x^{\text{tgt}} \leftarrow \mathcal{D}(z_0^{\text{tgt}})$ 21 $x^{\text{tgt}} \leftarrow \text{ColorTransfer}_{L^*a^*b^*}(x^{\text{piv}}, x^{\text{tgt}})$

with DPM-Solver [Lu et al. 2022]; of these, about 30 steps employ grounded self-attention. Inference results for this version are based on community checkpoints²³. For the FLUX [Labs 2024] version, we train a LoRA [Hu et al. 2022] of rank 128 using the Prodigy optimizer [Mishchenko and Defazio 2024] with learning rate 1 and total batch size 48. We also train this model for around 12K steps. At inference, we run 30 denoising steps with Euler [Karras et al. 2022]; of these about 18 steps employ grounded self-attention. Both models are trained at 512×512 resolution.

Baseline Details

22 return x^{tgt}

To introduce bokeh conditions in the pretrained T2I baselines, we append short descriptors to the text prompt. For the finetuned baselines, CSaT and GenPhoto, we follow their respective conditioning protocols, with some adaptations for fair comparison. CSaT [Fang et al. 2024] conditions generation on explicit camera intrinsics, such as aperture, focal length, and ISO. In our evaluation, we fix all parameters except aperture and vary only the F-number to control the

depth-of-field. According to the thin-lens equation (see main paper), the blur radius per unit disparity is inversely proportional to the fnumber. Therefore, we apply bokeh transitions in CSaT by adjusting aperture values inversely: for example, doubling the target bokeh strength corresponds to halving the F-number. GenPhoto [Yuan et al. 2024] shares the same defocus conditioning parameter as our method (blur radius in pixels per unit disparity). However, it is trained at a different image resolution. Since this parameter is defined in pixel space, we proportionally scale the bokeh values to ensure consistent visual blur across resolutions.

GPT-40 Evaluation

We leverage GPT-40 [OpenAI 2024] as a perceptual evaluator for two complementary metrics: bokeh accuracy and scene consistency. All evaluations are conducted via OpenAI's vision-language API, where images are passed alongside structured natural language instructions, and the model returns scalar outputs. We use a batchbased protocol, with images presented in context.

B.3.1 Bokeh accuracy. To assess how well the bokeh level in each image aligns with the intended defocus strength, we prompt GPT-40 to estimate a bokeh strength score for each image in a batch, within the given defocus blur range. The instruction used is as follows:

> We have several images below, each with a different bokeh strength. For each image, please provide a numeric bokeh strength score between 0 and {30}. A very low score means the image is in deep focus, while a high score means very strong defocus blur in the background. You should return only the scores and nothing else, in a single line, comma-separated, in the same order as the images.

The returned scores are then compared with the respective conditioning sequence using Pearson correlation to compute our GPTbased bokeh alignment metric.

B.3.2 Scene consistency. To evaluate how well a method preserves the underlying scene structure across varying bokeh levels, we present a batch of images and ask GPT-40 to provide a single scene consistency score. The instruction is:

> We have several images below of presumably the same scene but with varying depths-of-field. Please provide a single numeric score from 0 to 100 indicating how consistent the scene/subjects are across all these images, ignoring pure defocus blur differences but penalizing any other changes. A score of 100 means all images show precisely the same structure, while 0 means they're drastically changed in arrangement. Any minor variations in any of the images aside from bokeh should also be penalized. The only numeric score you should return is the scene consistency score.

This score serves as an additional perceptual consistency signal, complementing traditional metrics such as LPIPS.

 $^{^2} SG 161222 / Realistic_Vision_V 5.1$

³cyberdelia/CyberRealistic

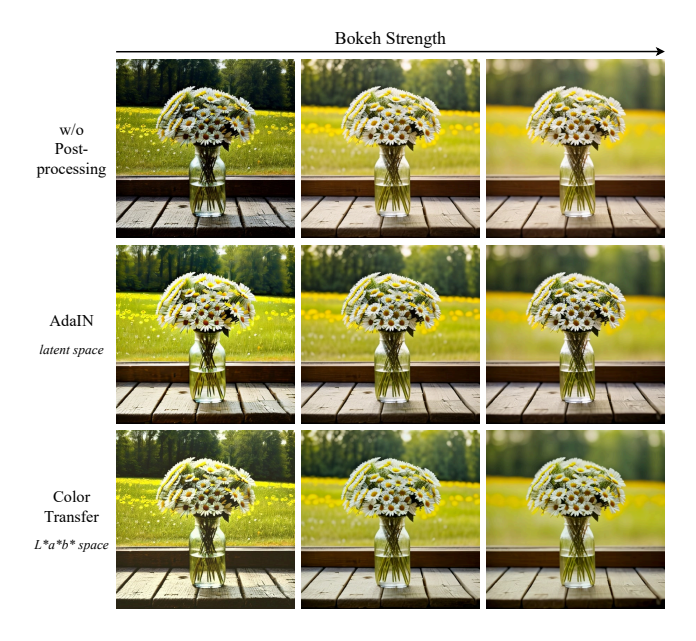


Fig. 15. Comparison of post-processing methods to mitigate color and lighting biases introduced by bokeh variation. Best viewed zoomed in.

C ADDITIONAL ABLATIONS

C.1 Image Color Transfer

As described in the main paper, a post-processing step is optionally applied to harmonize color and lighting across defocus levels. This helps mitigate subtle biases that can emerge when blur strength changes, especially under varying exposure in the training data. Figure 15 compares three versions of a target bokeh image: (1) without color transfer, (2) using AdaIN [Huang and Belongie 2017] in the latent space, and (3) using the method based on classic $L^*a^*b^*$ statistics matching [Reinhard et al. 2001]. While AdaIN effectively matches color and contrast to some extent, it also alters local variance (better noticeable in left column). In contrast, the $L^*a^*b^*$ -based method matches only the per-channel mean and variance in color space, leaving local detail structure and defocus effects intact. As a result, it preserves the intended depth-of-field while reducing color inconsistencies across scenes.

C.2 Grounding Steps

To study the impact of the number of grounding steps used during sampling, we perform an ablation on our FLUX-based model, which uses 30 total denoising steps. As shown in Fig. 16, the model is robust to a range of grounding configurations. Our default setting uses 18 grounding steps (60% of the sampling process), which mirrors the configuration used in the SD1.5 version and provides a good trade-off between scene consistency and flexible defocus control. Using too few grounding steps may lead to structural drift or inconsistencies in subject contours. Conversely, applying grounding for too many steps can overly constrain the model, occasionally resulting in artifacts when reducing blur or suppressing the achievable bokeh range when increasing it.

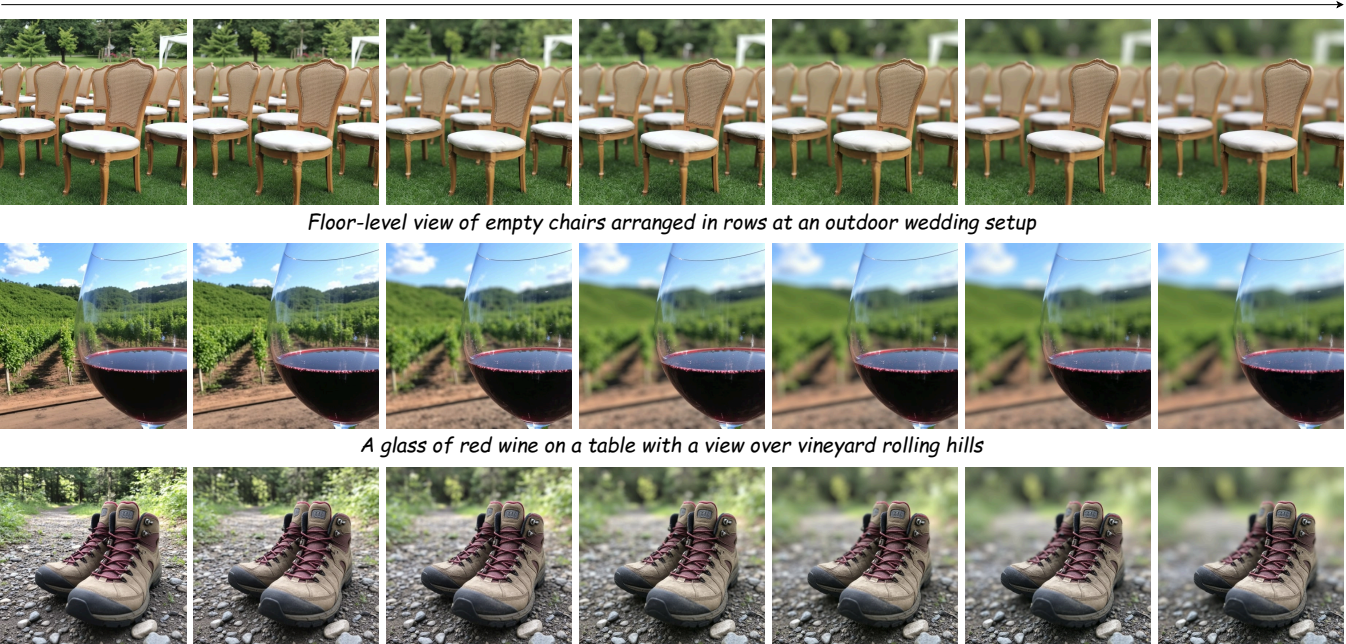
D ADDITIONAL VISUAL RESULTS

We provide additional qualitative results to highlight the versatility and consistency of Bokeh Diffusion under varying blur conditions. Fig. 17 illustrates a continuous progression of bokeh strength for a fixed scene, emphasizing the smooth, physically plausible control enabled by our method. Fig. 18 and Fig. 19 present more examples generated with our FLUX- and SD1.5-based models, respectively. We also show diverse unbounded bokeh control examples in Fig. 20 and Fig. 21. For dynamic visualizations, we encourage readers to view our project page, which includes video animations demonstrating continuous bokeh transitions across multiple scenes.



A vinyl record spins slowly on a turntable in a cozy living room, where morning sun casts long shadows across the rug Fig. 16. Effect of varying number of grounding steps during sampling in our FLUX-based model (out of 30 total).

Bokeh Strength



A pair of muddied hiking boots are left by a rocky trailhead with scattered pebbles and wildflowers growing nearby

Fig. 17. Continuous bokeh variation across fixed scenes. Our method allows smooth and physically grounded transitions between deep focus and shallow focus, producing consistent visual structure across intermediate blur levels.

Sharp Bokeh Sharp Bokeh A train track cutting through a valley A hawk perched on a fence post Ground-level shot of lit candles forming a trail up temple steps A car with a view of the city behind A woman using her phone while leaning Floor-level view of skateboards leaning on a wall against a colorful wall

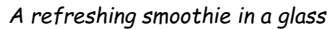
Fig. 18. Additional visual results for scene-consistent bokeh-conditioned generation from Bokeh Diffusion on FLUX [Labs 2024].

Ground-up view of umbrellas staked in sand along a beach

A classic motorcycle with a vintage style

Bokeh Sharp Sharp Bokeh A close-up of a kayak in a river A close shot of a deer in a snowy field A futuristic drone hovering silently, an urban skyline with digital overlays and twilight behind Rain-soaked alley glowing with neon reflections A close shot of a cow, farm behind A lantern glowing warmly on the porch at sunset







A close shot of a giraffe with a vast savannah behind

Fig. 19. Additional visual results for scene-consistent bokeh-conditioned generation from Bokeh Diffusion on SD1.5 [Rombach et al. 2022].



A close-up of a young man in casual attire, outdoor setting; bokeh 28



A close-up of a woman in a flower field; bokeh 22



A close shot of a cat, with a quiet garden behind; bokeh 30



A red kayak in a river; bokeh 0



A cute corgi puppy in a sunny backyard; bokeh 12



A surfboard at the beach; bokeh 2



A small bonsai tree in a pot, tranquil garden behind; bokeh 28



A close shot of a goat on a hill; bokeh 1



A rabbit in a forest; bokeh 18

Fig. 20. Additional visual results for unbounded bokeh-conditioned generation from Bokeh Diffusion on FLUX [Labs 2024].



A close shot of a car, city behind; bokeh 1



A smiling woman in a park with natural light behind; bokeh 18



A portrait of a man facing away in a busy street; bokeh 29



A seashell on the beach, gentle ocean waves in the background; bokeh 29



A cow on a farm; bokeh 14



A glass of red wine on a table with a view over vineyard rolling hills; bokeh 12



A refreshing smoothie with a market behind it; bokeh 0



A close shot of squirrel on a tree; bokeh 28



A close angle of a stack of golden pancakes drizzled with syrup; bokeh 28

Fig. 21. Additional visual results for unbounded bokeh-conditioned generation from Bokeh Diffusion on SD1.5 [Rombach et al. 2022].